Optics Letters

Broadband telecom photon pairs from a fiber-integrated PPLN ridge waveguide

Vikash Kumar Yadav,[1] Vivek Venkataraman,[1,2] and Joyee Ghosh[1,*]

[1]Department of Physics, Indian Institute of Technology Delhi, New Delhi 110016, India
[2]Department of Electrical Engineering, Indian Institute of Technology Delhi, New Delhi 110016, India
*Corresponding author: joyee@physics.iitd.ac.in

Received 29 July 2022; revised 12 September 2022; accepted 14 September 2022; posted 14 September 2022; published 27 September 2022

We demonstrate a spectrally correlated photon-pair source at telecom wavelengths (spanning across the S-, C-, and L-bands), based on type-0 spontaneous parametric down-conversion (SPDC) in a fiber-coupled Zn-indiffused MgO doped periodically poled lithium niobate (PPLN) ridge waveguide. Modal analysis of the waveguide performed through numerical finite element method (FEM) simulation indicates that device temperature can be used to dramatically vary and control the emission spectrum. Efficient photon-pair generation is measured over a broad wavelength range from ~1520 – 1580 nm [full width at half maximum (FWHM) > 45 nm] with a coincidence-to-accidental ratio (CAR) as high as ~668 and spectral brightness ~2.5×10^7 pairs/s/mW/nm. Such sources can be employed in wavelength division multiplexed (WDM) quantum key distribution (QKD) over existing fiber-optic networks.

https://doi.org/10.1364/OL.472045

Introduction. Sources based on spontaneous parametric down-conversion (SPDC) are widely used to generate spectrally uncorrelated and heralded single photons, spectrally correlated and entangled photon-pairs for various applications in quantum technology. In particular fiber-based applications employ telecom-band photons for key distribution [1], cryptography [2], and information processing [3]. Performance degradation due to chromatic dispersion in such critical applications can be mitigated via the use of spectrally correlated photon pairs [4–6]. With increasing experimental complexity in various state-of-the-art quantum communication protocols [7,8], the guided-wave approach seems to be promising in yielding compact, stable, and efficient photon sources [3,9,10]. Waveguide-based SPDC offers several advantages over bulk crystals, such as propagation of well-defined modes, enhancement of the effective nonlinearity due to strong confinement of optical modes, and efficient collection of the generated photons into single-mode fibers [11–13]. Here we report a fiber-integrated broadband source of spectrally correlated photon pairs at telecom wavelengths utilizing type-0 SPDC in a commercially available Zn-indiffused MgO doped periodically poled lithium niobate (PPLN) ridge waveguide. By demultiplexing the output into multiple wavelength channels using a standard telecom wavelength division multiplexed (WDM) device such as an arrayed waveguide grating (AWG), the same source can be used to serve multiple users in parallel for applications such as quantum metrology [9], quantum information processing [3], and quantum communication.

Numerical modal analysis of the waveguide. We employ a customized Zn-indiffused MgO:PPLN ridge waveguide (Covesion Ltd.), which is type-0 phase-matched (V → V + V, where V denotes vertical polarization) for the degenerate down-conversion process 775 nm (pump) → 1550 nm (signal) + 1550 nm (idler). The waveguide has a poling period of ~ 18.3 μm and is fabricated in z-cut (i.e., "z" denoting the optic-axis points in the vertical direction) MgO doped lithium niobate (MgO:LN) substrate. The schematic of the waveguide is shown in Fig. 1(a). The waveguide dimensions are height/depth (H) = 10 μm, width (W) = 10 μm, and length (L) = 4 cm. A Zn-indiffused waveguide offers high resistance to photorefractive damage, and guides both horizontal (H) and vertical (V) polarizations with a low propagation loss [14,15]. The change in the refractive index of MgO:LN due to Zn-indiffusion depends on the parameters of the diffusion process, such as Zn layer thickness and concentration, temperature, time, etc. [15,16]. The refractive index variation across the waveguide depth is shown in Fig. 1(b).

Numerical finite element method (FEM) simulation in COMSOL Multiphysics is used to extract the supported transverse magnetic (TM) modes (having V polarization) of this structure and the corresponding effective refractive indices (n_{eff}) at the phase-matched wavelengths. The material dispersion of MgO:LN is included using the Sellmeier equation [17], in which the refractive index is both wavelength and temperature dependent. The n_{eff} of the fundamental TM_{00} mode at 775 nm (pump) and 1550 nm (signal/idler) has near linear temperature dependence, as can be seen from the inset of Fig. 1(b). The waveguide is actually multimode at 775 nm (TM_{10} mode is also supported, not shown), but single-mode at the telecom wavelengths around 1550 nm. We note that the fundamental modes of both pump and signal/idler are well confined and near-circular, resulting in high mode overlap (~ 70.9%) and efficient coupling with single-mode fibers.

Phase-matching for type-0 SPDC. The SPDC process needs to satisfy energy conservation ($\omega_p = \omega_s + \omega_i$) and phase-matching constraints ($k_p = k_s + k_i$) where $\omega_{p,s,i}$ are the frequencies, while $k_{p,s,i}$ are the propagation vectors of the pump,

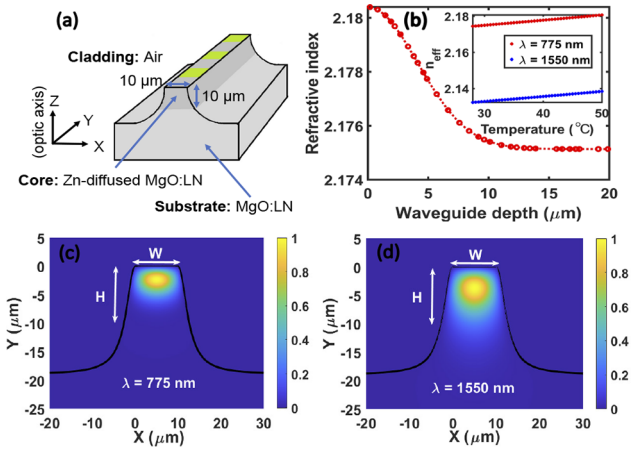

Fig. 1. (a) Schematic of a Zn-indiffused MgO:PPLN ridge waveguide. (b) Refractive index variation across the waveguide depth for 775 nm. Inset shows the n_{eff} versus temperature for 775 nm and 1550 nm. (c) Fundamental (TM_{00}) mode of the waveguide at 775nm. (d) TM_{00} mode at 1550 nm.

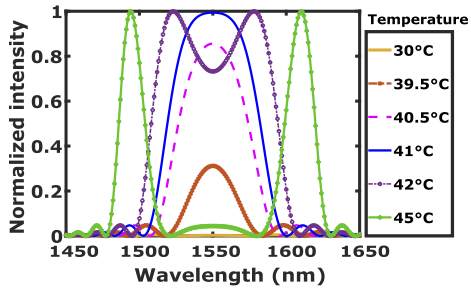

Fig. 2. Temperature dependence of the generated signal/idler spectra for λ_p = 775 nm.

signal, and idler, respectively. The type-0 SPDC in our device utilizes the largest second-order nonlinear susceptibility tensor component d_{33} = 25 pm/V [18] in LN. The material dispersion is compensated via quasi-phase-matching (QPM), where the crystal domains are inverted periodically, resulting in an effective nonlinear coefficient $d_{eff} = \frac{2}{\pi} d_{33}$. The net phase-mismatch (Δk) is then computed as [12,19]

$$\Delta k = \frac{2\pi}{\lambda_p}(n_{eff})_p - \frac{2\pi}{\lambda_s}(n_{eff})_s - \frac{2\pi}{\lambda_i}(n_{eff})_i - \frac{2\pi}{\Lambda}. \quad (1)$$

Here $\lambda_{p,s,i}$ are the wavelengths and $(n_{eff})_{p,s,i}$ are the effective refractive indices for pump, signal, and idler, respectively, and Λ is the poling period. We consider the Sellmeier equation [17] of the e-ray in MgO:LN in our simulation, since the waveguide is phase-matched for TM or V polarization (parallel to the optic-axis). In the continuous wave (CW) pump limit, the signal and idler spectra are determined solely by the phase-matching function $\mathrm{sinc}^2(\Delta kL/2)$ [3], where L is the length of the waveguide, and Δk is the phase-mismatch given by Eq. (1). Figure 2 shows the simulated signal/idler spectra at different temperatures.

The generated photon pairs have degenerate emission spectra below the phase-matching temperature (PMT) (T ~ 40.5 – 41°C), and non-degenerate spectra (non-overlapping discrete bands) above it. The phase-matching is quite broadband [>45nm full width at half maximum (FWHM) around 1550 nm center wavelength] at the phase-matching temperature. Further, both

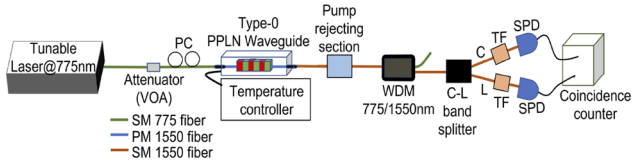

Fig. 3. Experimental setup of photon-pair generation: PC, polarization controller; SM, single-mode; PM, polarization maintaining; TF, tunable filter; SPD, single-photon detector. The pump rejecting section is implemented either using a free-space bandpass filter around 1550 nm or an in-line fiber-based long-pass filter that transmits wavelengths >1518 nm.

the shape and central wavelength of signal/idler spectra can be tuned over an extensive range with precise temperature control of the waveguide, keeping the pump wavelength constant.

Experimental characterization of telecom band photon-pair generation. The experimental setup for characterizing our source is shown in Fig. 3. The PPLN waveguide (Covesion Ltd.) device is pigtailed to polarization maintaining fiber (PM 1550) and packaged in a box with an oven inside to control the temperature. A CW tunable laser at 775 nm (Toptica Photonics AG) is used to pump the waveguide after controlling the power with a manual variable optical attenuator (VOA). The output from the PPLN device is passed through a bandpass filter (Thorlabs FB1550-40) to suppress the pump and transmit the telecom-band signal/idler photons. The bandpass filter has a FWHM bandwidth ~ 40 nm with insertion loss ≤ 1 dB at 1550 nm, while providing ~ 30 dB suppression at 775 nm. A customized WDM for 775/1550 nm which has a passband of 1550 ± 80 nm for the telecom port, is further used to filter out the telecom photons and reject the pump. The WDM has an insertion loss of 17 dB for pump and ≤ 1 dB at telecom. Thereafter, signal (short-wavelength) and idler (long-wavelength) photons are separated into two arms using a commercial C-L band splitter. The C-arm has a wavelength range of ~ 1500 – 1550 nm, and the L- arm of ~ 1550 – 1620 nm. Two single-photon avalanche photo detectors (SPAD) (Aurea Technology SPD_OEM_NIR) measure the photon counts in the C and L bands, each with a detection efficiency of 10%, dead time of 5 μs, and dark counts <1000 cps.

Figure 4(a) shows the dependence of the C and L band single-photon count rate on the device temperature and indicates a PMT ~ 41°C. The biphoton generation rate depends on the overlap integral of the pump, signal, and idler spatial modes [12,20]. The detected signal/idler photon count rate (R) can be computed as [20,21]

$$R \approx A \int \omega_s \omega_i f(\omega_s) \mathrm{sinc}^2(\Delta kL/2) \mathrm{d}\omega_s, \quad (2)$$

where constant A is a function of pump power, length of the waveguide, nonlinear coefficient, spatial overlap of pump, signal, and idler modes, etc. Here $f(\omega_s)$ is the filter function, which is given as $f(\omega_s) = B(\omega_s)C(\omega_s)$ for C-band photon count rate and $f(\omega_s) = B(\omega_s)L(\omega_s)$ for L-band photon count rate. Again $B(\omega_s)$ is the bandpass filter (used for pump rejection) transmission function, $C(\omega_s)$ is the C-band transmission function and $L(\omega_s)$ is the L-band transmission function of the C-L band splitter. The solid curve, shown in Fig. 4(a) is plotted using Eq. (2).

The signal/idler photon generation rate is maximum at the degenerate SPDC phase-matching temperature, and nearly follows a sinc^2 dependence on temperature, as shown in Fig. 4(a).

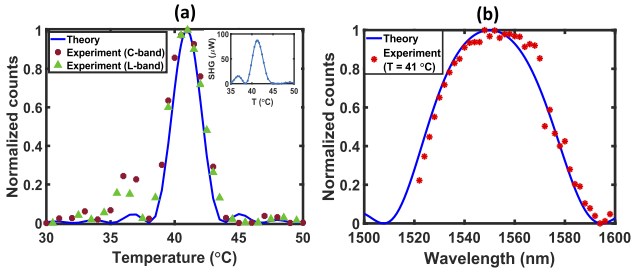

Fig. 4. (a) Dependence of SPDC single-photon count rate on the temperature of the waveguide. The solid line represents the theoretical variation, and the dots show the experimental result through the C-arm and L-arm of the C-L band splitter. Inset shows the measured SHG versus temperature of the waveguide indicating PMT = 41°C and SHG efficiency ~ 30%/W. (b) Single-photon (signal/idler) counts versus tunable filter wavelength at the phase-matching temperature.

The theoretical prediction is in good agreement with the experimental results, especially for the main central lobe. The slight asymmetry and larger sidelobes in our experimental data could be due to inhomogeneous Zn doping along the length and/or the non-uniformity of the width and/or poling period of the waveguide [22], and fabrication limits of the waveguides [23].

Bandwidth measurement. For bandwidth characterization of the source, the fiber-coupled broadband SPDC output is filtered via a narrowband digital tunable filter (FWHM bandwidth of 1.2 nm) to detect photons at a particular wavelength. The pump rejecting section, C-L band splitter and coincidence counter are not used in this experiment; the tunable filter is connected just after the 775/1550 WDM to detect the single photons. We tune the digital filter center wavelength across the C- and L-bands (from ~ 1520 – 1620 nm) and measure the photon counts at the phase-matching temperature of the waveguide. The raw detected photon counts are adjusted by the wavelength-dependent insertion-loss profile of the digital tunable filter to yield the data shown in Fig. 4(b). The experimental data show a good agreement with the theory [$\mathrm{sinc}^2(\Delta kL/2)$]. The emission bandwidth of our source is thus measured to be ~ 46 nm (FWHM) centered at 1550 nm.

Spectral correlation measurement through joint spectral intensity. Measurement of the joint spectral intensity (JSI) unveils the generated biphoton frequency correlation [12]. JSI with a circular or horizontally/vertically oriented elliptical shape represents spectrally uncorrelated photons, which is desired for heralded single-photon sources. Whereas a negatively inclined elliptical JSI represents spectrally correlated photons, which is desired for entanglement-based quantum key distribution [4,12] and other quantum information applications. The two-photon output state of a source is computed as [24]

$$|\psi\rangle = B \iint f(\omega_s, \omega_i)\hat{a}^\dagger(\omega_s)\hat{a}^\dagger(\omega_i)|0\rangle_s|0\rangle_i \mathrm{d}\omega_s \mathrm{d}\omega_i, \quad (3)$$

where B is the spatial overlap of pump, signal, and idler modes. Here $\hat{a}^\dagger(\omega_s)$ and $\hat{a}^\dagger(\omega_i)$ are the creation operators for signal and idler photons, respectively. The function $f(\omega_s, \omega_i)$ is the two-photon amplitude, i.e., joint spectral amplitude (JSA) that describes the spectrum of generated signal/idler photons. Here $|f(\omega_s, \omega_i)|^2$ is the JSI [12,25], which can be written as

$$|f(\omega_s, \omega_i)|^2 = |\alpha(\omega_s, \omega_i)|^2 |\phi(\omega_s, \omega_i)|^2, \quad (4)$$

where $\alpha(\omega_s, \omega_i)$ is the input pump spectrum, i.e., pump envelope function, and $\phi(\omega_s, \omega_i)$ is the phase matching function.

The pump envelop function for a pulsed source (assuming a Gaussian shape) is defined as $\alpha(\omega_s, \omega_i) = \exp\left(-\left(\frac{\omega_s+\omega_i-\omega_p}{\sigma_p}\right)^2\right)$ [12,24] where ω_p is the central pump frequency, and σ_p is the pump spectral bandwidth. For a CW source $\alpha(\omega_s, \omega_i)$ can be approximated as a Dirac delta function. The phase-matching function is given as $\phi(\omega_s, \omega_i) = \mathrm{sinc}\left(\frac{\Delta kL}{2}\right)\exp\left(\frac{-i\Delta kL}{2}\right)$. To measure the JSI we implement the pump rejecting section in Fig. 3 using an in-line long-pass filter which has transmission from 1518 nm to 1620 nm and pump the waveguide with ~ 24.5 μW at 775 nm.

We record the coincidence counts for each (λ_s, λ_i) pair by stepping through the entire signal and idler wavelength range in discrete steps of 1 nm. We first fix the signal arm filter at one wavelength, scan the whole idler wavelength range, and then increase the signal filter wavelength and repeat the same process. The measured JSI is shown in Fig. 5(a), which is negatively inclined at −45° indicating a strong spectral correlation between signal and idler photons. It is evident that a signal photon at one wavelength is correlated with only its partner idler photon that fulfills the energy conservation condition, with negligible single-photon fluorescence present in the coincidence spectra.

Coincidence-to-accidental ratio. CAR gives a measure of the quality of a biphoton source, i.e., the temporal correlation between the generated signal/idler photons [26]. The peak coincidence rate measured at zero time delay between the two output photons (C_t) is known as "true coincidences", while the background coincidence rate at any finite time delay (larger than the measurement bin-width and/or the coherence time of the biphotons) (C_a) is known as "accidental coincidences". The ratio of these two is defined as CAR = C_t/C_a [10]. Accidental coincidences can arise due to some background flu-

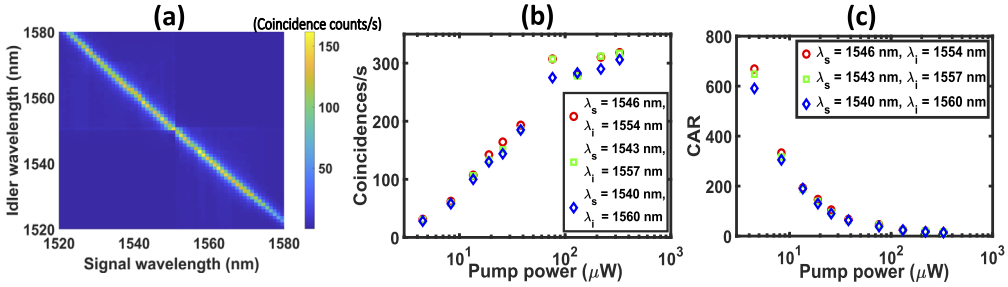

Fig. 5. (a) The joint spectral intensity of a type-0 Zn-indiffused MgO:PPLN waveguide at phase-matching temperature. (b) Coincidence count rate as a function of the pump power for three different signal/idler channels. (c) The coincidence-to-accidental ratio (CAR) as a function of pump power for three different signal/idler channels.

Table 1. Comparison of Photon-Pair Sources in Telecom Band: PPLN/W (Waveguide), PPLN/C (Crystal)

Source	Spectral Brightness (pairs/s/mW/GHz)	Bandwidth (nm)	CAR
PPLN/W [27]	Not reported	50	300
PPLN/W [10]	Not reported	36	4138
PPLN/C [28]	Not reported	132	40
PPLN/W [9]	1.96×10^6	40	NR
Our source	2×10^5	46	668

orescence/scattering process, multi-photon generation events, detector dark counts and/or pump photons leaking through the optical components. CAR is an important figure of merit to estimate how many undesired noise photons are being generated along with the desired photons. A high CAR value ensures good quality/purity of the correlated photon-pair source.

We fix the tunable filter of signal and idler in Fig. 3 at three different wavelength pairs and increase the pump (775 nm) power to record the coincidence and CAR as shown in Figs. 5(b) and 5(c). The true CAR is calculated by subtracting the coincidences due to dark counts from C_t and C_a in the CAR defined above. We observe that the coincidence rate increases with increased pump power, but the CAR value reduces drastically. This trade-off can be explained by the fact that an increase in pump power also increases the accidental counts along with the true coincidences, since more pump photons can now leak through the optical components, and the probability of multi-photon generation also increases. We measure a CAR value as high as 668, indicating the high purity of our source. We also observe a CAR>1300 when complete C- and L-bands were passed into the detectors, i.e., without tunable filters. After factoring out all external losses and detector efficiencies, we estimate the internal spectral brightness of our source as $\approx 2.5 \times 10^7$ generated photon pairs/s/mW/nm.

Conclusion. We have demonstrated a fiber-integrated broadband (FWHM ~ 46 nm) source of spectrally correlated photon pairs at telecom wavelengths, spanning the S-, C-, and L-bands. Table 1 lists the details of a comparison of our source with some previously reported type-0 PPLN based photon-pair sources in telecom band. A negatively inclined JSI and high CAR value (>650) show the high quality (large spectral and temporal correlations) of our source. We believe that such sources could be potential candidates for quantum metrology, and WDM based multi-user quantum key distribution (QKD) applications over existing fiber-optic networks.

Funding. Department of Science and Technology, Ministry of Science and Technology, India (DST/ICPS/QuST/Theme-1/2019/Q-62).

Acknowledgments. The research fellowship of V.K.Y. was supported by the Council of Scientific and Industrial Research, India.

Disclosures. The authors declare no conflicts of interest.

Data availability. Data underlying the results presented in this paper are not publicly available at this time but may be obtained from the authors upon reasonable request.

REFERENCES

1. D. Aktas, B. Fedrici, F. Kaiser, T. Lunghi, L. Labonté, and S. Tanzilli, Laser Photonics Rev. **10**, 451 (2016).
2. T. Jennewein, C. Simon, G. Weihs, H. Weinfurter, and A. Zeilinger, Phys. Rev. Lett. **84**, 4729 (2000).
3. J. Chen, A. J. Pearlman, A. Ling, J. Fan, and A. Migdall, Opt. Express **17**, 6727 (2009).
4. T. Lutz, P. Kolenderski, and T. Jennewein, Opt. Lett. **39**, 1481 (2014).
5. O. Kuzucu, M. Fiorentino, M. A. Albota, F. N. C. Wong, and F. X. Kärtner, Phys. Rev. Lett. **94**, 083601 (2005).
6. A. Gajewski and P. Kolenderski, Phys. Rev. A **94**, 013838 (2016).
7. X.-M. Jin, J.-G. Ren, B. Yang, Z.-H. Yi, F. Zhou, X.-F. Xu, S.-K. Wang, D. Yang, Y.-F. Hu, S. Jiang, T. Yang, H. Yin, K. Chen, C.-Z. Peng, and J.-W. Pan, Nat. Photonics **4**, 376 (2010).
8. F. B. Basset, M. Valeri, E. Roccia, V. Muredda, D. Poderini, J. Neuwirth, N. Spagnolo, M. B. Rota, G. Carvacho, F. Sciarrino, and R. Trotta, Sci. Adv. **7**, eabe6379 (2021).
9. P. Vergyris, F. Kaiser, E. Gouzien, G. Sauder, T. Lunghi, and S. Tanzilli, Quantum Sci. Technol. **2**, 024007 (2017).
10. S. Arahira, N. Namekata, T. Kishimoto, H. Yaegashi, and S. Inoue, Opt. Express **19**, 16032 (2011).
11. S. Tanzilli, H. De Riedmatten, H. Tittel, S. Tanzilli, H. de Riedmatten, W. Tittel, H. Zbinden, P. Baldi, M. de Micheli, D. B. Ostrowsky, and N. Gisin, Electron. Lett. **37**, 26 (2001).
12. R. Kumar and J. Ghosh, J. Opt. **20**, 075202 (2018).
13. R. Kumar, V. K. Yadav, and J. Ghosh, Phys. Rev. A **102**, 033722 (2020).
14. W. M. Young, R. S. Feigelson, M. M. Fejer, M. J. F. Digonnet, and H. J. Shaw, Opt. Lett. **16**, 995 (1991).
15. W. Young, M. Fejer, M. Digonnet, A. Marshall, and R. Feigelson, J. Lightwave Technol. **10**, 1238 (1992).
16. S. A. Berry, L. G. Carpenter, A. C. Gray, P. G. R. Smith, and C. B. E. Gawith, OSA Continuum **2**, 3456 (2019).
17. O. Gayer, Z. Sacks, E. Galun, and A. Arie, Appl. Phys. B **91**, 343 (2008).
18. W. P. Risk, T. R. Gosnell, and A. V. Nurmikko, *Compact Blue-Green Lasers* (Cambridge University Press, 2003).
19. R. W. Boyd, *Nonlinear Optics* (Academic Press, 2020).
20. J. Schneeloch, S. H. Knarr, D. F. Bogorin, M. L. Levangie, C. C. Tison, R. Frank, G. A. Howland, M. L. Fanto, and P. M. Alsing, J. Opt. **21**, 043501 (2019).
21. M. Fiorentino, S. M. Spillane, R. G. Beausoleil, T. D. Roberts, P. Battle, and M. W. Munro, Opt. Express **15**, 7479 (2007).
22. A. C. Gray, S. A. Berry, L. G. Carpenter, J. C. Gates, P. G. R. Smith, and C. B. E. Gawith, IEEE Photonics Technol. Lett. **32**, 63 (2020).
23. M. Santandrea, M. Stefszky, V. Ansari, and C. Silberhorn, New J. Phys. **21**, 033038 (2019).
24. C. K. Law, I. A. Walmsley, and J. H. Eberly, Phys. Rev. Lett. **84**, 5304 (2000).
25. A. Christ, K. Laiho, A. Eckstein, T. Lauckner, P. J. Mosley, and C. Silberhorn, Phys. Rev. A **80**, 033829 (2009).
26. H. Takesue and K. Inoue, Opt. Express **13**, 7832 (2005).
27. M. Hunault, H. Takesue, O. Tadanaga, Y. Nishida, and M. Asobe, Opt. Lett. **35**, 1239 (2010).
28. H. Kim, O. Kwon, and H. S. Moon, Sci. Rep. **9**, 5031 (2019).